Dalton Transactions

ROYAL SOCIETY OF CHEMISTRY

PAPER

View Article Online
View Journal | View Issue

Cite this: *Dalton Trans.*, 2025, **54**, 966

pK_a of alcohols dictates their reactivity with reduced uranium-substituted thiomolybdate clusters†

Kamaless Patra, William W. Brennessel and Ellen M. Matson *

Received 6th October 2024,
Accepted 20th November 2024

DOI: 10.1039/d4dt02803a

rsc.li/dalton

The uranium-substituted thiomolybdate cluster, **(Cp*$_3$Mo$_3$S$_4$)UCp***, has been demonstrated as a model for water reduction by single uranium atoms supported on a molybdenum sulfide surface (U@MoS_2). In this study, the scope of O–H bond activation is expanded through the investigation of the reactivity of various alcohols with differing pK_a values for the –OH proton. The reaction of **(Cp*$_3$Mo$_3$S$_4$)UCp*** with stoichiometric amounts of methanol, phenol, 2,6-dichlorophenol, and nonafluoro-*tert*-butyl alcohol affords the corresponding mono-alkoxide species, **(Cp*$_3$Mo$_3$S$_4$)Cp*U(OR)**, *via* a uranium-metalloligand cooperative activation of the O–H bond. This observed reactivity is analogous to the O–H bond activation reported by **(Cp*$_3$Mo$_3$S$_4$)UCp*** in the presence of water. However, addition of *tert*-butanol induces protonolysis of the Cp* ligand on uranium, resulting in the formation of a uranium tris-*tert*-butoxide cluster, **(Cp*$_3$Mo$_3$S$_4$)U(O^{t}Bu)$_3$**. Independent synthesis of **(Cp*$_3$Mo$_3$S$_4$)Cp*U(O^{t}Bu)** was possible *via* an alternative pathway, eliminating sterics as a justification for the observed discrepancy in reactivity. These results offer insight into the role the –OH proton pK_a plays in dictating the mechanism of O–H bond activation of alcohols by the uranium-substituted thiomolybdate cluster.

Introduction

Actinide compounds have gained increased prominence in the catalysis of a wide range of chemical transformations.[1,2] The origins of this interest trace back to 1905, when atomically dispersed uranium and uranium nitride were utilized for the conversion of N_2 to ammonia.[3] This unique reactivity, driven by uranium's large ionic radius, redox activity, and the involvement of diffuse 5f orbitals in bonding, continues to open new avenues in the activation of small molecules.[4,5–10] Moreover, the development of uranium catalysts for small molecule activation reactions plays an important role in the development of uses of depleted uranium remaining from the front-end processing of materials for nuclear technologies.[11–13]

Recently, the combination of uranium and redox non-innocent ligands has emerged as an appealing strategy for enabling multielectron reactivity at the actinide center.[14–26] In these complexes, redox active ligands act as an electron reservoir, stabilizing actinide centres in low formal oxidation states. These complexes have shown considerable promise in the activation of small molecules, including organic azides, azo compounds, CO_2, CO, and H_2O.[16,27–35]

Despite significant progress of small molecule activation at low-valent uranium, the reports of reactivity toward the activation of –OH groups in water and alcohols, particularly those focused on controlled stoichiometric reactivity leading to the release of H_2, remain limited.[30,36,37] The importance of investigating this reactivity stems from recent advancements in electrocatalytic hydrogen evolution reactions (HER) with water. In this context, Meyer and co-workers have reported the water reduction catalysis with U(III) complex ([[((Ad,Me)ArO)$_3$*mes*)U]), highlighting the precise role of uranium–ligand (arene) δ bonding cooperativity in the key steps of the catalytic cycle.[32]

Another promising approach for leveraging the unique reactivity of actinide centres *via* cooperative interactions with their coordination sphere involves the installation of the 5f-elements on reducible, heterogeneous surfaces. The interaction between the redox-active surface and the actinide introduces the potential for multi-electron transformations.[4] For example, single uranium atom centres deposited on MoS_2 nanomaterials have been demonstrated as effective electrocatalysts for HER from water.[35] This study demonstrates the crucial role of actinide-surface cooperativity in O–H bond activation. Notably, DFT calculations suggest that the sulfur centre

Department of Chemistry, University of Rochester, Rochester, NY, 14627, USA. E-mail: matson@chem.rochester.edu

†Electronic supplementary information (ESI) available: ^{1}H NMR spectra for all compounds **(Cp*$_3$Mo$_3$S$_4$)Cp*U(OR)** (R = Me, Ph, $PhCl_2$, $C(CF_3)_3$), **(Cp*$_3$Mo$_3$S$_4$)Cp*U(OPh)$_2$**, **(Cp*$_3$Mo$_3$S$_4$)U(O^{t}Bu)$_3$**, and selected crystallographic parameters for complexes **(Cp*$_3$Mo$_3$S$_4$)Cp*U(OR)** (R = Me, $PhCl_2$), **(Cp*$_3$Mo$_3$S$_4$)Cp*U(OPh)$_2$**, and **(Cp*$_3$Mo$_3$S$_4$)U(O^{t}Bu)$_3$**. CCDC 2388772–2388775. For ESI and crystallographic data in CIF or other electronic format see DOI: **https://doi.org/10.1039/d4dt02803a**

on the MoS_2 surface abstracts a hydrogen atom from water, releasing it as hydrogen, while the oxygen centre is bound to uranium.[35] Similar involvement of sulfido moieties in HER has been described for other molecular catalysts based on metal chalcogenides, which models the active sites of MoS_2 materials.[38,39–41]

Our group is investigating the electronic structure and reactivity of a reduced, uranium-substituted thiomolybdate cluster, **(Cp*$_3$Mo$_3$S$_4$)UCp*** (Fig. 1).[30,42] The isolation and structural analysis of a wide range of **(Cp*$_3$Mo$_3$S$_4$)Cp*U(X)$_n$** (X = –I, –OH, =NR; n = 1, 2) clusters provide additional insight into how surface interactions are influenced by the oxidation/reduction processes of the cluster, as well as the effects of ligand addition to the uranium centre. In the context of water reduction, our team has demonstrated that upon addition of H_2O, reduction of the substrate occurs, resulting in the formation of uranium-hydroxide species, **(Cp*$_3$Mo$_3$S$_4$)Cp*U(OH)$_n$** (n = 1, 2), that closely resemble the molecular form of intermediates invoked in HER at U@MoS_2. Moreover, mechanistic studies have demonstrated a metal–ligand cooperative pathway for O–H bond activation of water across the uranium–sulfur bond.

In this study, the reactivity of the **(Cp*$_3$Mo$_3$S$_4$)UCp*** cluster toward a series of alcohols is described (Fig. 1). The addition of an equivalent of methanol, phenol derivatives, or nonafluoro-*tert*-butanol leads to the cooperative activation of the O–H bond across the uranium-cluster surface, resulting in the formation of corresponding uranium mono-alkoxide species along with the liberation of H_2. A change in reactivity was observed as a function of the pK_a of the alcohol –OH group; as the pK_a increases, protonolysis of the Cp* ligand occurs as a competitive side reaction. In the case of *tert*-butanol, which has high pK_a for –OH proton, the alcohol reacts with reduced cluster to liberate Cp*H. Overall, the study presents a pK_a-dependent cooperative reactivity of alcohol with the uranium-substituted thiomolybdate cluster.

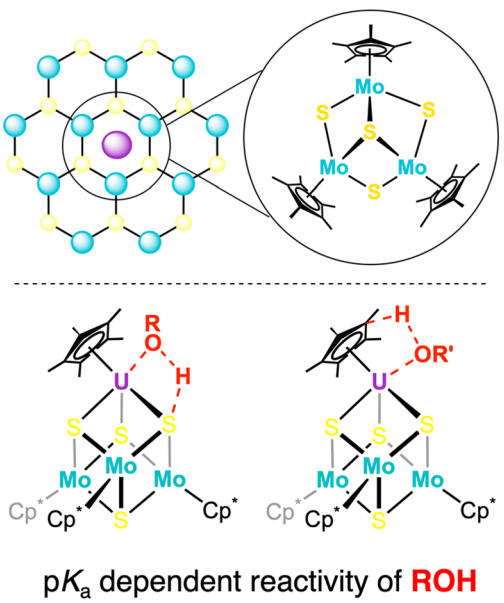

Fig. 1 Cooperative O–H bond activation by a reduced, uranium-substituted thiomolybdate cluster, **(Cp*$_3$Mo$_3$S$_4$)UCp***. Current work demonstrates pK_a dependent reactivity of O–H bonds at the low-valent uranium centre.

Experimental

Safety considerations

Caution! Depleted uranium (primary isotope ^{238}U) is a weak α-emitter (4.197 MeV) with a half-life of 4.47×10^9 years. Due to the short half-lives of daughter nuclei, *e.g.* 234-Th (27 days) and 234-Pa (1.1 minutes), all but the most recently purified uranium will also emit a small amount of beta radiation. As such, manipulations and reactions should be carried out in monitored fume hoods or in an inert atmosphere drybox in a radiation laboratory equipped with α- and β-counting equipment.

General considerations

All air- and moisture-sensitive manipulations were carried out using standard high vacuum line, Schlenk, or cannula techniques, or in an MBraun inert atmosphere drybox containing and atmosphere of purified dinitrogen. Solvents for air- and moisture-sensitive manipulations were dried and deoxygenated using a Glass Contour Solvent Purification System (Pure Process Technology, LLC) and stored over activated 4 Å molecular sieves (Fisher Scientific) prior to use. Deuterated solvents for ^{1}H NMR spectroscopy were purchased from Cambridge Isotope Laboratories and stored in the glovebox over activated 3 Å molecular sieves after three freeze–pump–thaw cycles. Alcohols were purified by conventional methods, distilled under nitrogen, and deoxygenated prior to use. A 0.1 M stock solution of all alcohols was prepared in anhydrous toluene; this stock solution was then diluted to 0.05 M and deoxygenated again before being added to the cluster. **(Cp*$_3$Mo$_3$S$_4$)UCp*** [42] was synthesized following established procedures.

Physical measurements

^{1}H NMR spectra were recorded at room temperature on a 400 MHz Bruker AVANCE spectrometer locked on the signal of deuterated solvents. All the chemical shifts are reported relative to the chosen deuterated solvent as a standard. Elemental analysis data were obtained from the Elemental Analysis Facility at the University of Rochester. Microanalysis samples were weighed with a PerkinElmer model AD6000 Autobalance, and their compositions were determined with a PerkinElmer 2400 Series II analyser. Air-sensitive samples were handled in a VAC glovebox.

Single crystal X-ray crystallography

Single crystals of **(Cp*$_3$Mo$_3$S$_4$)Cp*U(OMe)**, **(Cp*$_3$Mo$_3$S$_4$)Cp*U(OPh^{Cl2})**, **(Cp*$_3$Mo$_3$S$_4$)Cp*U(OPh)$_2$**, **(Cp*$_3$Mo$_3$S$_4$)U(O^{t}Bu)$_3$** were placed on a nylon loop and mounted on a Rigaku XtaLAB Synergy-S Dualflex diffractometer equipped with a HyPix-

6000HE HPC area detector for data collection at 100.00(10) K (Table S1†). A preliminary set of cell constants and an orientation matrix were calculated from a small sampling of reflections. A short pre-experiment was run, from which an optimal data collection strategy was determined. The full data collection for all four complexes was carried out using a PhotonJet (Cu) X-ray source. Absorption corrections based on carefully-measured crystal faces were applied. The final cell constants were calculated from the *xyz* centroids of the strong reflections from the actual data collections after integration. The structure was solved using SHELXT[43] and refined using SHELXL.[44] Most or all non-hydrogen atoms were assigned from the solution. Full-matrix least-squares/difference Fourier cycles were performed, which located any remaining non-hydrogen atoms. All the non-hydrogen atoms were refined with anisotropic displacement parameters. All the hydrogen atoms were placed in ideal positions and refined as riding atoms with relative isotropic displacement parameters.

General procedure for the synthesis of $(Cp^*_3Mo_3S_4)Cp^*U(OR)$

A 20 mL scintillation vial was charged with **$(Cp^*_3Mo_3S_4)UCp^*$** (0.020 g, 0.017 mmol) and 5 mL of toluene and kept at −30 °C for 10 minutes. In a separate vial, a solution of alcohol in toluene (0.05 M, 0.34 mL) was prepared. The alcohol solution was added dropwise to the cold solution of **$(Cp^*_3Mo_3S_4)UCp^*$**, with swirling of the solution after each addition. The solvent was removed immediately following the addition of alcohol under reduced pressure. The resultant residue was subsequently redissolved in toluene and filtered through a pipette containing filter paper to eliminate insoluble substances. Volatiles were removed under reduced pressure, resulting in the isolation of the title compounds, **$(Cp^*_3Mo_3S_4)Cp^*U(OR)$** (R = Me, Ph, Cl_2Ph), as black powders.

Characterization data for $(Cp^*_3Mo_3S_4)Cp^*U(OMe)$

Yield = 0.019 g, 0.016 mmol, 94%; ^{1}H NMR (400 MHz, C_6D_6) δ = 108.05 (135, 3H, C*H*$_3$), 5.86 (60, 45H, MoC$_5$*Me*$_5$), −5.20 (72, 15H, UC$_5$*Me*$_5$); anal. calcd for $C_{41}H_{63}Mo_3S_4UO$ (mol. wt 1226.073 g mol^{-1}): C, 40.16%; H, 5.18%. Found: C, 40.51%; H, 5.20%. Crystals suitable for single crystal X-ray diffraction (SCXRD) were grown from the concentrated toluene/THF (10 : 1) solution of the title compound at −30 °C.

Characterization data for $(Cp^*_3Mo_3S_4)Cp^*U(OPh)$

Yield = 0.021 g, 0.016 mmol, 94%; ^{1}H NMR (400 MHz, C_6D_6) δ = 29.21 (66, 2H, Ph–*H*), 18.74 (60, 2H, Ph–*H*), 14.93 (55, 1H, Ph–*H*), 5.48 (56, 45H, MoC$_5$*Me*$_5$), −2.79 (52, 15H, UC$_5$*Me*$_5$); anal. calcd for $C_{46}H_{65}Mo_3S_4UO{\cdot}(C_7H_8)_{0.25}$ (mol. wt 1288.144 g mol^{-1}): C, 43.74%; H, 5.15%. Found: C, 43.66%; H, 5.20%.

Characterization data for $(Cp^*_3Mo_3S_4)Cp^*U(OPh^{Cl2})$

Yield = 0.022 g, 0.016 mmol, 94%; ^{1}H NMR (400 MHz, C_6D_6) δ = 12.10 (41, 2H, Ph–*H*), 10.62 (39, 1H, Ph–*H*), 5.57 (51, 45H, MoC$_5$*Me*$_5$), 1.33 (46, 15H, UC$_5$*Me*$_5$); anal. calcd for $C_{46}H_{63}Mo_3S_4UOCl_2{\cdot}(C_7H_8)_{1.2}$ (mol. wt 1357.028 g mol^{-1}): C, 44.52%; H, 4.99%. Found: C, 44.72%; H, 5.08%. Crystals suitable for SCXRD were grown from the concentrated toluene solution of the title compound at −30 °C.

Characterization data for $(Cp^*_3Mo_3S_4)Cp^*U(OC(CF_3)_3)$

Yield = 0.022 g, 0.015 mmol, 91%, ^{1}H NMR (400 MHz, C_6D_6) δ = 8.12 (38, 15H, UC$_5$*Me*$_5$), 4.21 (51, 45H, MoC$_5$*Me*$_5$); ^{19}F{^{1}H} NMR (C_6D_6): δ = −87.15 (s, CF_3); anal. calcd for $C_{44}H_{60}Mo_3S_4UOF_9{\cdot}(C_7H_8)$ (mol. wt 1430.068 g mol^{-1}): C, 40.24%; H, 4.50%. Found: C, 40.30%; H, 4.25%.

Reaction of $(Cp^*_3Mo_3S_4)UCp^*$ with 1.1 equiv. of phenol

A 20 mL scintillation vial was charged with **$(Cp^*_3Mo_3S_4)UCp^*$** (0.030 g, 0.025 mmol) and 5 mL of toluene. In a separate vial, a solution of phenol (2.6 mg, 0.027 mmol) in toluene (0.1 ml) was prepared. This alcohol solution was added to the **$(Cp^*_3Mo_3S_4)UCp^*$** solution in a single step at room temperature. The solvent was immediately removed under reduced pressure following the addition of phenol, and the residue was subsequently redissolved in toluene. The resulting toluene solution was filtered through a pipette containing filter paper to remove insoluble substances. Volatiles were then removed under reduced pressure, yielding the crude product as a black powder. ^{1}H NMR analysis suggest a mixture of products (Fig. S6†).

Synthesis of $(Cp^*_3Mo_3S_4)Cp^*U(OPh)_2$

A 20 mL scintillation vial was charged with **$(Cp^*_3Mo_3S_4)Cp^*U(OPh)$** (0.020 g, 0.015 mmol) and 5 mL of toluene and kept at −30 °C for 10 minutes. In a separate vial, a solution of phenol in toluene (0.05 M, 0.3 mL) was prepared. The phenol solution was added dropwise to the cold solution of **$(Cp^*_3Mo_3S_4)Cp^*U(OPh)$**, with swirling of the solution gently after each addition. The resulting toluene solution was filtered through a pipette containing filter paper immediately after the addition of phenol to remove insoluble substances. The solvent was then evaporated. The crude product was washed with pentane (3 × 5 mL) and evaporated, yielding the title compound **$(Cp^*_3Mo_3S_4)Cp^*U(OPh)_2$** as a black powder. Yield = 0.015 g, 0.011 mmol, 73%, ^{1}H NMR (400 MHz, C_6D_6) δ = 12.49 (66, 4H, Ph–*H*), 9.17 (60, 4H, Ph–*H*), 8.43 (55, 2H, Ph–*H*), 6.72 (56, 45H, MoC$_5$*Me*$_5$), 2.17 (52, 15H, UC$_5$*Me*$_5$). Black crystals of **$(Cp^*_3Mo_3S_4)Cp^*U(OPh)_2$** suitable for SCXRD were grown from the concentrated toluene solution of the title compound at −30 °C. Anal. calcd for $C_{52}H_{70}Mo_3S_4UO_2$ (mol. wt 1381.249 g mol^{-1}): C, 45.22%; H, 5.11%. Found: C, 45.40%; H, 5.21%.

Alternative synthesis

$(Cp^*_3Mo_3S_4)UCp^*$ (0.020 g, 0.017 mmol) was treated with two equivalents of phenol (0.05 M, 0.7 mL) following the same procedure as the first pathway. After a similar workup, **$(Cp^*_3Mo_3S_4)Cp^*U(OPh)_2$** was obtained as a black powder. Yield = 0.016 g, 0.011 mmol, 67%.

H_2 gas measurement

The experiment was performed in a J-young NMR tube. The tube was sequentially charged with the C_6D_6 solution of

(Cp*$_3$Mo$_3$S$_4$)UCp* (0.4 ml), blank C_6D_6 (0.2 ml), and the C_6D_6 solution of alcohol (0.2 ml), freezing the solution after each addition. Finally, the frozen mixture was capped, and as it began to thaw, it was inserted into the NMR spectrometer. The immediate formation of the product and the evolution of H_2 gas are detected in the ^{1}H NMR spectrum.

Synthesis of (Cp*$_3$Mo$_3$S$_4$)U(O^{t}Bu)$_3$

A 20 mL scintillation vial was charged with **(Cp*$_3$Mo$_3$S$_4$)UCp*** (0.020 g, 0.017 mmol) and 5 mL of toluene and kept at −30 °C for 10 minutes. In a separate vial, a solution of *tert*-butanol in toluene (0.05 M, 1.0 mL) was prepared. The alcohol solution was added dropwise to the cold solution of **(Cp*$_3$Mo$_3$S$_4$)UCp***, with swirling of the solution gently after each addition. The solution was left overnight without any stirring. Then, the solvent was removed under reduced pressure and subsequently redissolved in toluene. The resulting toluene solution was filtered through a pipet containing filter paper to eliminate insoluble substances before being evaporated, yielding the title compound **(Cp*$_3$Mo$_3$S$_4$)U(O^{t}Bu)$_3$** as a black powder. Yield = 0.023 g, 0.016 mmol, 95%, ^{1}H NMR (400 MHz, C_6D_6) δ = 6.26 (52, 45H, MoC$_5$*Me*$_5$), 1.77 (46, 27H, ^{t}Bu–*H*). Brown crystals of ([Cp*$_3$Mo$_3$S$_4$]Cp*U(O^{t}Bu)$_3$) suitable for SCXRD were grown from the concentrated toluene solution of the title compound at −30 °C. Anal. calcd for $C_{42}H_{72}Mo_3S_4UO_3$ (mol. wt 1212.046 g mol^{-1}): C, 39.44%; H, 5.67%. Found: C, 39.13%; H, 5.48%.

Synthesis of (Cp*$_3$Mo$_3$S$_4$)Cp*U(O^{t}Bu)

A 20 mL scintillation vial was charged with **(Cp*$_3$Mo$_3$S$_4$)UCp*** (0.020 g, 0.017 mmol) and 5 mL of toluene. The solution was cooled to −30 °C in a freezer. Addition of a solution of di-*tert*-butyl peroxide (0.05 M, 0.17 mL) was performed, following the same procedure as that of the synthesis of **(Cp*$_3$Mo$_3$S$_4$)Cp*U(OR)**. The solvent was removed immediately following the addition of the peroxide under reduced pressure and subsequently redissolved in toluene. The resulting toluene solution was filtered through a pipette containing filter paper to eliminate insoluble substances. Volatiles were removed under reduced pressure, resulting in the isolation of the title compounds, **(Cp*$_3$Mo$_3$S$_4$)Cp*U(O^{t}Bu)**, as black powders. Yield = 0.020 g, 0.016 mmol, 92%, ^{1}H NMR (400 MHz, C_6D_6) δ = 36.65 (40, 9H, ^{t}Bu–*H*), 4.51 (50, 45H, MoC$_5$*Me*$_5$), −3.26 (42, 15H, UC$_5$*Me*$_5$). Anal. calcd for $C_{44}H_{69}Mo_3S_4UO$ (mol. wt 1268.154 g mol^{-1}): C, 41.67%; H, 5.48%. Found: C, 41.95%; H, 5.51%.

Results and discussion

Reactivity of (Cp*$_3$Mo$_3$S$_4$)UCp* toward alcohols

Following our recent studies on cooperative O–H bond activation of water by the reduced uranium-substituted thiomolybdate cluster, **(Cp*$_3$Mo$_3$S$_4$)UCp***,[30] we sought to expand the scope of uranium-metalloligand cooperativity in the activation of O–H bonds in other substrates. Since this reaction mechanism involves the transfer of an H-atom from the substrate following coordination to the actinide-substituted thiomolybdate cluster, we became interested in understanding the dependence of the pK_a of the O–H group on product selectivity and H_2 production. Toward this goal, **(Cp$_3$*Mo$_3$S$_4$)UCp*** was treated with one equivalent of methanol (Scheme 1).

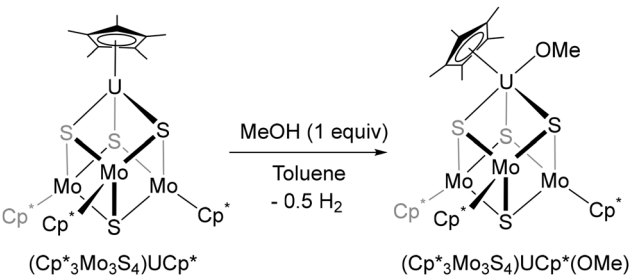

Scheme 1 Synthesis of **(Cp*$_3$Mo$_3$S$_4$)Cp*U(OMe)**.

Our interest in this primary alcohol stems from its relatively high pK_a value for the –OH group compared to water. Upon addition of methanol to the reduced uranium-substituted thiomolybdate cluster, a colour change from dark brown to blue-green was observed.

The ^{1}H NMR spectrum of the crude reaction mixture reveals complete conversion of the actinide-containing starting material to a single product (Fig. 2 and Fig. S1†). The product exhibits a downfield shift of the Cp*-methyl protons on molybdenum (5.85 ppm, 45H) and uranium (−5.21 ppm, 15H) centres compared to those in the starting material; the observed chemical shifts resemble values reported for (Cp*$_3$Mo$_3$S$_4$)Cp*U(OH).[30] A signal located at 108.05 ppm is

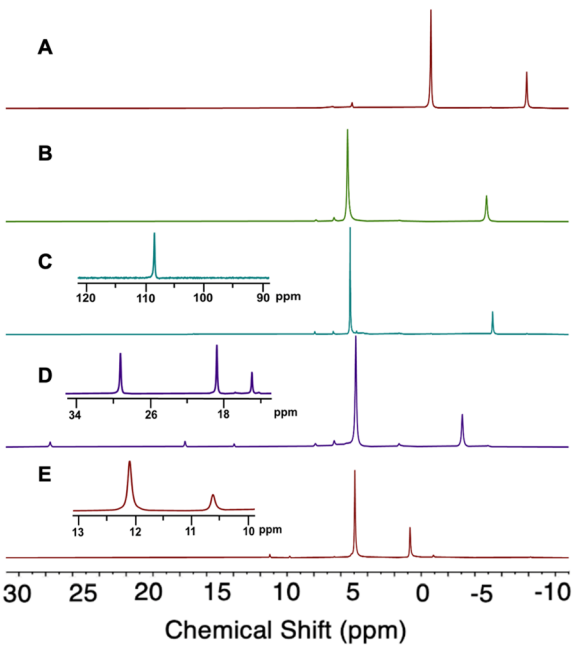

Fig. 2 ^{1}H NMR spectra of (A) **(Cp*$_3$Mo$_3$S$_4$)UCp***, (B) **(Cp*$_3$Mo$_3$S$_4$)Cp*U(OH)**, (C) **(Cp*$_3$Mo$_3$S$_4$)Cp*U(OMe)**, (D) **(Cp*$_3$Mo$_3$S$_4$)Cp*U(OPh)**, and (E) **(Cp*$_3$Mo$_3$S$_4$)Cp*U(OPh^{Cl2})** in C_6D_6 at room temperature. Insets: The respective alkoxide signals of **(Cp*$_3$Mo$_3$S$_4$)Cp*U(OR)** in spectrum C, D, and E.

assigned to the methyl protons of U–OCH_3; this assignment was made based upon integrations of the resonances, as well as similarities of the chemical shift of the methoxide protons to those reported for the uranium mono-methoxide compound, [($^{t\text{-Bu}}$ArO)$_3$tacnU^{IV}(OMe)].[45] To support formation of mono-methoxide compound, the reactivity was further investigated with deuterated substrate; addition of CD_3OD to an equivalent of **(Cp*$_3$Mo$_3$S$_4$)UCp*** was performed in a J-Young tube containing proteo benzene. The U–OCD_3 signal was detected in the ^{2}H NMR spectrum, resonating at 115.74 ppm (Fig. S4†). The formation of D_2 was also observed in the ^{2}H NMR spectrum (Fig. S5†). Based on these data, the product of methanol addition to **(Cp$_3$*Mo$_3$S$_4$)UCp*** was tentatively assigned as the uranium mono-methoxide species, **(Cp*$_3$Mo$_3$S$_4$)Cp*U(OMe)**.

Dark crystals obtained from the crude reaction mixture of **(Cp*$_3$Mo$_3$S$_4$)UCp*** and methanol were analysed by single-crystal X-ray diffraction (SCXRD). Upon refinement of the data, unambiguous confirmation of the formation of the mono-methoxide cluster **(Cp$_3$Mo$_3$S$_4$)Cp*U(OMe)** (Fig. 3 and Table 1; see Table S1† for structural parameters) was obtained. The coordination environment of the uranium centre contains a single methoxide substituent, an η^5-Cp* ligand, and the three sulfide atoms composing the face of the hemicubane thiomolybdate scaffold. The U–O distance of 2.104(6) Å closely resembles that of the mono-hydroxide species [(Cp$_3$Mo$_3$S$_4$)Cp*U(OH)] (2.123(5) Å). In addition, the U–O distance and the C–O–U angle (161.5(6)°) are in good agreement with values reported for uranium(IV) mono-methoxide compounds [U–O = 2.027(2) Å, ∠U–O–C = 161.3(2)°, [U(tpa)I$_3$(OMe)]; U–O = 2.100(6) Å (R = ^{t}Bu), U–O = 2.097(4) Å (R = Ad); [((^{R}ArO)$_3$tacn)U^{IV}(OMe)]].[45,46]

The Mo–μS_U (avg) (μS_U = μ-S coordinated to uranium) distance is 2.405(5) Å, consistent with that observed in analogous mono-hydroxide (2.403(4) Å) and mono-iodide (2.403(2) Å) species. A similar U–S_{surf} (S_{surf} = centroid of the three μ_2-bridged sulfur atoms) distance of 1.721(1) Å compared to that of the single electron oxidized mono-hydroxide species (1.709(1) Å) suggests a comparable interaction of uranium with the trisulfide surface of the hemicubane in both complexes. This distance is shorter compared to the analogous two-electron oxidized cluster (*e.g.*, U–S_{surf} = 1.8622 (9) Å in (Cp*$_3$Mo$_3$S$_4$)Cp*U(OH)$_2$,[30] U–S_{surf} = 1.8554(6) Å in (Cp*$_3$Mo$_3$S$_4$)Cp*UI$_2$,[42] and U–S_{surf} = 1.899(1) Å in (Cp*$_3$Mo$_3$S$_4$)Cp*U(OPh)$_2$, *vide infra*). This suggests that oxidation of the cluster leads to a weakening of the uranium's interaction with the trisulfide surface. This trend is consistent with reports of analogous transition metal-

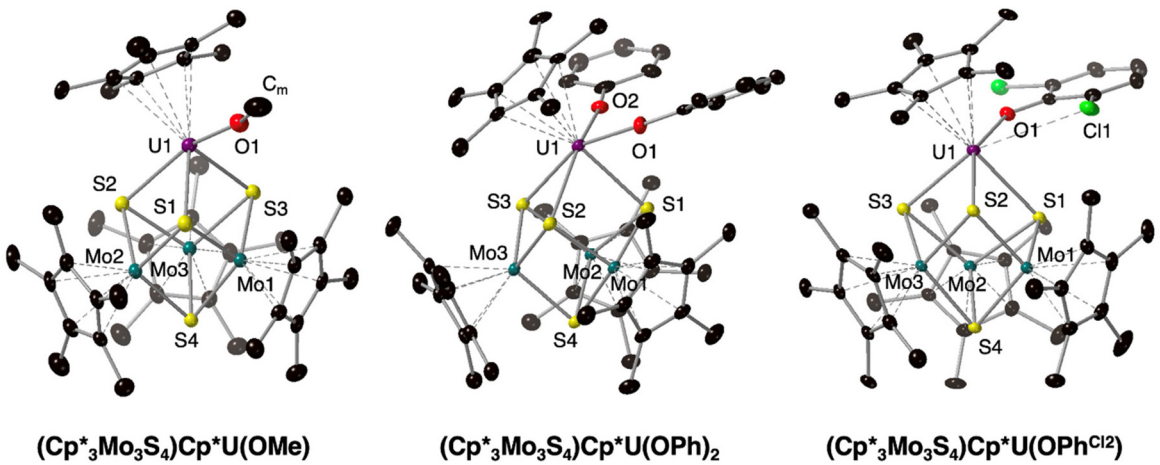

Fig. 3 Molecular structures of **(Cp*$_3$Mo$_3$S$_4$)Cp*U(OMe)** (left), **(Cp*$_3$Mo$_3$S$_4$)Cp*U(OPh)$_2$** (middle), and **(Cp*$_3$Mo$_3$S$_4$)Cp*U(OPh^{Cl2})** (right) are shown with 40% probability ellipsoids. Hydrogen atoms and solvent molecules have been removed for clarity. Key: black, C; red, O; yellow, S; green, Cl; teal, Mo; purple, U.

Table 1 Pertinent bond distances and angles of **(Cp*$_3$Mo$_3$S$_4$)Cp*U(OMe)**, **(Cp*$_3$Mo$_3$S$_4$)Cp*U(OPh)$_2$**, **(Cp*$_3$Mo$_3$S$_4$)U(OPh^{Cl2})** and **(Cp*$_3$Mo$_3$S$_4$)U(O^{t}Bu)$_3$**

Bond	(Cp*$_3$Mo$_3$S$_4$)Cp*U(OMe)	(Cp*$_3$Mo$_3$S$_4$)Cp*U(OPh)$_2$	(Cp*$_3$Mo$_3$S$_4$)U(OPh^{Cl2})	(Cp*$_3$Mo$_3$S$_4$)U(O^{t}Bu)$_3$
U–C_{Cp^*} (Å)	2.755(8)–2.846(8)	2.787(6)–2.821(7)	2.759(4)–2.805(4)	—
U–Cp^*_{cent} (Å)	2.520(4)	2.525(3)	2.509(2)	—
U–O (Å)	2.104(5)	2.141(4), 2.153(4)	2.235(3)	2.092(3), 2.080(3), 2.089(3)
U–S (Å)	2.638(2), 2.681(2), 2.759(2)	2.735(2), 2.797(2), 2.852(2)	2.6430(9), 2.6912(9), 2.7195(9)	2.7252(8), 2.7371(8), 2.7558(8)
Mo–S_U (avg) (Å)	2.405(5)	2.374(4)	2.401(2)	2.385(4)
Mo–S_{Mo} (avg) (Å)	2.330(3)	2.320(3)	2.332(2)	2.325(1)
Mo···Mo (Å)	2.8880(8), 2.8919(8), 2.6725(8)	2.7620(7), 2.9054(7), 2.8627(7)	2.9206(4), 2.8813(4), 2.6816(4)	2.7299(4), 2.8488(4), 2.8458(3)
U–S_{surf} (Å)	1.721(1)	1.899(1)	1.7036(6)	1.8208(7)
∠U–O–C	161.5(6)°	157.0(4)°, 167.6(4)°	144.3(3)°	157.9(3)°, 162.2(2)°, 157.4(3)°

based heterometallic cubane clusters (*e.g.*, Ti–S_{surf} = 1.2297(4) Å in $Cp^*_3Mo_3S_4TiCl_2$ *vs.* Ti–S_{surf} = 1.066(1) Å in the reduced form $[K(THF)_2]_2[Cp^*_3Mo_3S_4Ti]_2(\mu\text{-}N_2)$).[47] Similarly, molecular complexes of uranium [((^{Ad,Me}ArO)$_3$*mes*)U], featuring δ-bonding interactions with the arene ring surface, as reported by Meyer and co-workers, have also shown a weakening of the interaction upon oxidation of the uranium center (U–$arene_{Cent}$ = 2.35 Å in [{(^{Ad,Me}ArO)$_3$mes}U] and U–$arene_{Cent}$ = 2.18 Å in [[{(^{Ad,Me}ArO)$_3$mes}U]K(2,2,2 cryptant)]).[48]

Multiple synthetic pathways have been reported for the generation of cyclopentadienyl uranium alkoxide complexes. One widely used approach involves the alcoholysis of Cp/Cp* or amide ligands on uranium, though this method typically yields uranium bis- and tris-alkoxide complexes.[49] Another method is the salt metathesis reaction with corresponding uranium halides, which is particularly effective with bulky alkoxides.[50] In contrast to these approaches, the reduction of alcohol offers an atom-economic approach to access uranium mono-alkoxides, with hydrogen as the only by-product. Meyer and co-workers have previously reported a similar synthetic route for the synthesis of uranium mono-alkoxide compounds.[45] The formation of **(Cp*$_3$Mo$_3$S$_4$)Cp*U(OMe)** following addition of methanol to the reduced uranium-substituted thiomolybdate cluster constitutes the second example of this synthetic approach for the formation of uranium-alkoxide moieties.

The reactivity of **(Cp*$_3$Mo$_3$S$_4$)UCp*** with phenol was next explored. This substrate has a more acidic –OH proton than methanol and water (Scheme 2). Surprisingly, the reaction of **(Cp*$_3$Mo$_3$S$_4$)UCp*** with ∼1.1 equivalents of phenol afforded a mixture of products, as observed in the ^{1}H NMR spectrum, with concurrent release of H_2 (Fig. S6,† see the Experimental section for details). The major product possesses a set of signals with chemical shifts of 5.47 ppm (45 H, Mo–Cp*) and −2.80 ppm (15 H, U–Cp*) for the Cp* protons. Additional resonances were observed at 29.20 (2 H), 18.73 (2 H), and 14.91 ppm (1 H), consistent with the formation of a uranium mono-phenoxide compound, **(Cp*$_3$Mo$_3$S$_4$)Cp*U(OPh)** (further discussion of ^{1}H NMR spectrum is provided below). The minor set of signals exhibited downfield-shifted Cp* resonances at 6.72 ppm (45 H, Mo–Cp*) and 2.17 ppm (15 H, U–Cp*), with phenyl ring protons at 12.50 (4 H), 9.17 (4 H), and 8.46 ppm (2 H). Based on relative integrations of these assigned signals, it was hypothesized that this minor component corresponds to the bis-phenoxide species, **(Cp*$_3$Mo$_3$S$_4$)Cp*U(OPh)$_2$**. The downfield shift of the Cp* protons, compared to the mono-methoxide species, aligns with expectations for a two-electron oxidized compound. Moreover, they closely resemble the shifts observed in the analogous bis-hydroxide species, **(Cp*$_3$Mo$_3$S$_4$)Cp*U(OH)$_2$**.[30]

Independent synthesis of **(Cp*$_3$Mo$_3$S$_4$)Cp*U(OPh)$_2$** was accomplished *via* the addition of 2 equivalents of phenol to **(Cp*$_3$Mo$_3$S$_4$)UCp*** (Scheme 2; see the Experimental section for details; Fig. S7†). Crystals grown from this reaction mixture were analysed by SCXRD (Fig. 3 and Table 1; see Table S1† for structural parameters). The molecular structure of **(Cp*$_3$Mo$_3$S$_4$)Cp*U(OPh)$_2$** reveals the coordination environment of the uranium centre is composed of two phenoxide moieties, the η^5-Cp* ligand, and the three sulphide atoms of the face of the hemi-cubane scaffold. The U–O bond distances in **(Cp*$_3$Mo$_3$S$_4$)Cp*U(OPh)$_2$** are 2.141(4) and 2.153(4) Å, while the U–O–C angles are 157.0(4)° and 167.6(4)°. Both the U–O bond distances and U–O–C angles closely match those observed for the mono-methoxide compound, suggesting that the electronic effects of the alkoxide ligand do not significantly alter the U–O bonding and geometrical disposition. In addition, both parameters closely resemble those of reported uranium(IV)-phenoxide compounds, such as [Cp*U(OPh)(HN_3^{Mes})], (U–O = 2.147(9) Å); (Cp^*_2U(O-2,6-^{i}Pr$_2$-C_6H_3)(CH_3), (U–O = 2.126(4) Å); (UI_2(O-4-^{t}BuC_6H_4)$_2$(THF)$_3$, (U–O = 2.051(8), 2.084(8) Å)), with U–O–C angles ranging from 163.2(4)° to 165.4(6)°).[51–53] A notable shortening of the Mo–μS_U (avg) distance is observed upon the addition of a second alkoxide ligand to uranium (from 2.405(5) to 2.374(4) Å), which is consistent with the oxidation of the metalloligand. The interaction between the uranium center and the trisulfide surface of the hemicubane is also investigated by measuring the distance between the uranium center and the centroid of the three μ_2-bridged sulfur

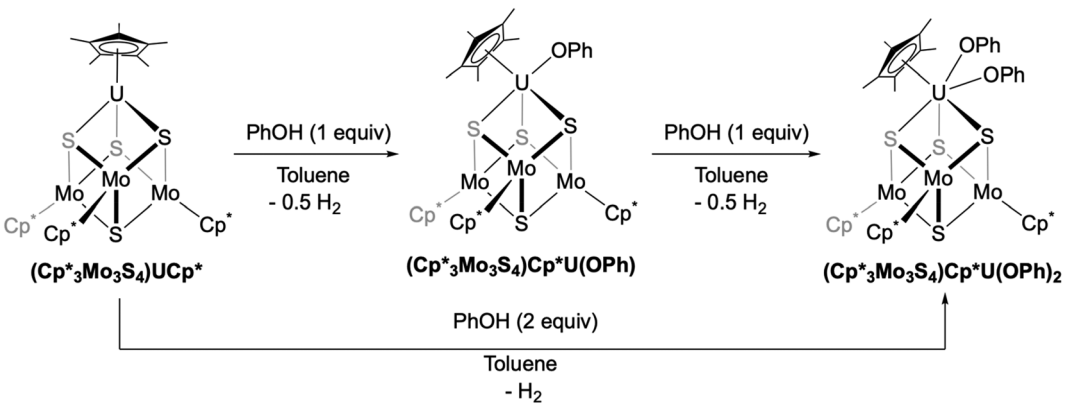

Scheme 2 Synthesis of **(Cp*$_3$Mo$_3$S$_4$)Cp*U(OPh)** and **(Cp*$_3$Mo$_3$S$_4$)Cp*U(OPh)$_2$**.

atoms (S_{surf}) in $Cp^*_3Mo_3S_4$, which is 1.899(1) Å. The elongation in U–S_{surf} distance from that observed in the mono-methoxide species is consistent with the general trend that oxidation results in lengthening and weakening of these interactions (*vide supra*). It is worth noting that the U–S_{surf} distance closely resembles that observed in $(Cp^*_3Mo_3S_4)Cp^*U(OH)_2$ (1.8622(9) Å).

To avoid the formation of a mixture of mono- and bis-phenoxide species, the reaction was conducted with phenol under more precise conditions, allowing the desired mono-phenoxide compound to be obtained separately and cleanly (Scheme 2). A dilute toluene solution of exactly 1 equivalent of phenol was added dropwise to the toluene solution of **$(Cp_3{}^*Mo_3S_4)UCp^*$**. This time, ^{1}H NMR spectroscopy of the crude product revealed the formation of a single product. The signals attributed to the methyl protons of Mo–Cp* (5.47 ppm, 45 H) and U–Cp* (−2.80 ppm, 15 H) were shifted downfield in comparison to the starting material, indicating cluster oxidation (Fig. 2 and Fig. S8†). However, these signals were shifted upfield relative to those observed for **$(Cp_3{}^*Mo_3S_4)Cp^*U(OPh)_2$**. The methyl protons of Mo–Cp* resonated similarly to those of **$(Cp_3{}^*Mo_3S_4)Cp^*U(OMe)$**, whereas U–Cp* was shifted downfield. This downfield shift of U–Cp* is likely due to the electron-withdrawing nature of the phenoxide substituent compared to methoxide. Additional resonances were observed at 29.20 (2 H), 18.73 (2 H), and 14.91 (1 H) ppm, which were assigned to a single phenoxide ligand bound to the uranium centre following the activation of one equivalent of phenol. Although the crystal structure of the mono-phenoxide species remains elusive, elemental analysis confirms the formation of **$(Cp^*_3Mo_3S_4)Cp^*U(OPh)$**.

Notably, the addition of a further equivalent of phenol to **$Cp^*_3Mo_3S_4UCp^*(OPh)$** results in conversion to the bis-phenoxide product **$(Cp^*_3Mo_3S_4)Cp^*U(OPh)_2$**, as confirmed by ^{1}H NMR spectroscopy (Scheme 2 and Fig. S9†). This observation further validates the existence of **$(Cp^*_3Mo_3S_4)Cp^*U(OPh)$**.

The formation of the bis-phenoxide product stimulated curiosity in the reactivity of multiple equivalents of methanol with the reduced uranium-substituted thiomolybdate cluster. As such, the reactivity of multiple equivalents of methanol and **$(Cp^*_3Mo_3S_4)UCp^*$** was explored. It was hypothesized that the differing pK_a of the –OH proton in methanol compared to phenol might influence the second O–H bond activation. The addition of 2 equivalents of methanol to **$(Cp^*_3Mo_3S_4)UCp^*$** under conditions analogous to those of the reaction with 1 equivalent was explored. The ^{1}H NMR spectrum of the reaction mixture, however, does not show the anticipated downfield shift for the Cp*-methyl protons on molybdenum and uranium, which would typically indicate a two-electron oxidation of the cluster and the formation of a uranium bis-methoxide species. Instead, the spectrum reveals a mixture of products, with new signals appearing at 1.97 ppm and 18.10 ppm, alongside the starting mono-methoxide cluster (Fig. S10†). Protonolysis of the Cp* ligand is also evident in the ^{1}H NMR spectrum. The intensity ratio of two signals at 1.97 and 18.10 ppm (15 : 45) suggests the formation of a uranium containing product with an empirical formula of **$(Cp^*_3Mo_3S_4)U(OMe)_5$**. The possibility of the product being an ion pair, **$[(Cp^*_3Mo_3S_4)^+U(OMe)_5^-]$**, cannot be ruled out, as the chemical shift of the Cp*-methyl protons resembles that observed for the cationic form of the metalloligand **$[(Cp^*_3Mo_3S_4)PF_6]$** (2.01 ppm).[54] Indeed, high-valent uranium centres dissociating from the cluster have also been reported in earlier studies.[30]

The addition of a third equivalent of methanol to **$(Cp^*_3Mo_3S_4)UCp^*$** increased the intensity of the signals attributed to Cp*H and the proposed uranium pentamethoxide species, while reducing the intensity of the starting mono-methoxide compound (Fig. S11†). Based on these findings, we hypothesize that, after the single-electron oxidation of the reduced cluster, the S-centre of the mono-alkoxide species becomes less basic, requiring a more acidic proton to liberate hydrogen through U–S cooperative activation of the O–H bond. This result supports the crucial role of the pK_a of the –OH proton of alcohol in influencing the second O–H bond activation.

The scope of reactivity was expanded by employing 2,6-dichlorophenol, a substrate with a more acidic –OH proton than that of phenol (Scheme 3).[55] We were particularly interested in the *o*-chloro derivative, hypothesizing that the *o*-chloro substituent could engage in a non-bonding interaction with uranium. This interaction might facilitate the crystallization of the mono-phenoxide species by preventing the formation of the bis-phenoxide, effectively blocking the site required for binding a second substrate. Treatment of **$(Cp^*_3Mo_3S_4)UCp^*$** with 2,6-dichlorophenol results in the formation of a single product, as observed in the ^{1}H NMR spectrum (Fig. 2 and Fig. S12†). The Mo–Cp* and U–Cp* methyl protons resonate at 5.57 and 1.33 ppm, respectively, while the phenyl ring protons are paramagnetically shifted and resonate at 12.11 and 10.61 ppm. The U–Cp* methyl protons are shifted downfield compared to those of the mono-methoxide and mono-phenoxide compounds, likely due to the electron-withdrawing nature of the dichlorophenoxide ligand. The intensity ratio of the phenyl ring protons to the Cp* protons suggests the formation of the mono-dichlorophenoxide uranium species.

Confirmation of the formation of the purported mono-dichlorophenoxide compound was achieved *via* SCXRD. Dark, needle-shaped crystals were obtained from a concentrated toluene solution of **$(Cp^*_3Mo_3S_4)Cp^*U(OPh^{Cl2})$** at −30 °C (Fig. 3

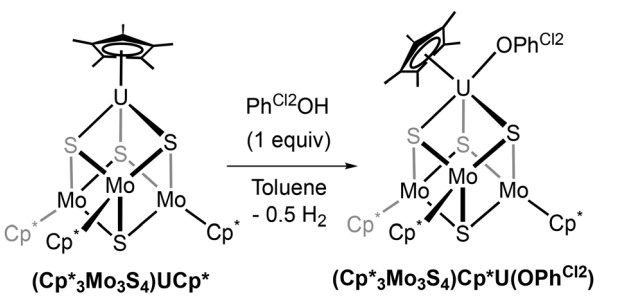

Scheme 3 Synthesis of **$(Cp^*_3Mo_3S_4)Cp^*U(OPh^{Cl2})$**.

and Table 1; see Table S1† for structural parameters). The molecular structure reveals that the coordination environment of the uranium center consists of the η^5-Cp* ligand, three sulfide centers forming the face of the hemicubane metalloligand, and a new 2,6-dichlorophenoxide ligand. The U–O bond distance in **$(Cp^*_3Mo_3S_4)Cp^*U(OPh^{Cl2})$** is elongated (2.235(3) Å) in comparison to those observed in bis-phenoxide and mono-methoxide species, which can be attributed to the non-bonding interaction between the *o*-chloro substituent on the phenyl ring and the uranium center (3.367(1) Å). This interaction likely causes the U–O–C bond angle (144.3(3)°) to be smaller compared to those in the bis-phenoxide and mono-methoxide species. Additionally, the interaction of the *o*-chloro substituent renders the phenyl ring more electron-deficient, withdrawing electron density from the adjacent oxygen atom and thereby weakening the U–O bond. In contrast, a slight shortening and strengthening of the U–Cp* bond (U–Cp^*_{cent} = 2.509(2) Å) in **$(Cp^*_3Mo_3S_4)Cp^*U(OPh^{Cl2})$** is observed compared to the corresponding bis-phenoxide complex (2.525(3) Å) and mono-methoxide species (2.520(4) Å). The U–S (2.6430(9)–2.7195(9) Å) and U–S_{surf} (1.7036(6) Å) distances in **$(Cp^*_3Mo_3S_4)Cp^*U(OPh^{Cl2})$** are shorter than those observed in the two-electron oxidized **$(Cp^*_3Mo_3S_4)Cp^*U(OPh)_2$** species (U–S: 2.735(2) to 2.852(2) Å; U–S_{surf} = 1.899(1) Å). However, these distances closely resemble those of the mono-methoxide species (U–S: 2.64(2)–2.762(2) Å; U–S_{surf} = 1.721(1) Å).

We further attempted the reaction of **$(Cp^*_3Mo_3S_4)Cp^*U(OPh^{Cl2})$** with an additional equivalent of 2,6-dichlorophenol or phenol to form the bis-alkoxide species. However, no immediate reaction was observed with either substrate. This observation suggests that uranium most likely requires an open coordination site for the second O–H bond activation to occur.

To further assess the influence of the –OH proton's pK_a, the reactivity was explored by employing *tert*-butanol as a substrate (Scheme 4). *tert*-Butanol possesses a less acidic –OH group than the other alcohols in this study.[56] Interestingly, the reaction of **$(Cp^*_3Mo_3S_4)UCp^*$** with one equivalent of *tert*-butanol showed no immediate reaction, as observed using ^{1}H NMR spectroscopy. This lack of reactivity was intriguing, given that alcohol reduction of all other substrates occurs immediately.

However, a few hours after the addition of *tert*-butanol to the reduced cluster, a new product signal appeared with approximately 30% conversion, accompanied by the liberation of Cp*H (Fig. S13†). Based on these observations, we hypothesized the formation of a uranium alkoxide species with no Cp* ligand on uranium with the formula, **$(Cp^*_3Mo_3S_4)U(O^tBu)_x$**. The intensity ratio of two new sets of signals (45 : 27) aligns with the proposed species **$(Cp^*_3Mo_3S_4)U(O^tBu)_3$**. The Cp*-methyl protons on molybdenum resonate at 6.26 ppm, and the *tert*-butyl protons resonate at 1.77 ppm. We note that another set of signals corresponding to a minor product in the reaction mixture appear at 4.51, −3.26, and 36.65 ppm with an intensity ratio of 45 : 15 : 9. These signals closely resemble those of the analogous mono-methoxide species, **$(Cp^*_3Mo_3S_4)Cp^*U(OMe)$**. Integrations of all resonances suggest a product ratio of **$(Cp^*_3Mo_3S_4)U(O^tBu)_3$** to **$(Cp^*_3Mo_3S_4)Cp^*U(O^tBu)$** of 5 : 1.

To confirm the stoichiometry based on ^{1}H NMR, we sought to synthesize the **$(Cp^*_3Mo_3S_4)U(O^tBu)_3$** independently using three equivalents of substrate (Scheme 4). Consequently, the reaction of three equivalents of *tert*-butanol with **$(Cp^*_3Mo_3S_4)UCp^*$** consumed all the starting material and resulted in the formation of a single product, **$(Cp_3Mo_3S_4)U(O^tBu)_3$**, along with the removal of 1 equivalent of Cp*H (Fig. S14 and S15†), as evidenced from ^{1}H NMR spectrum.

Unambiguous confirmation of **$(Cp^*_3Mo_3S_4)U(O^tBu)_3$** was performed by SCXRD. Dark brown, needle-shaped crystals were grown from the concentrated toluene solution of **$(Cp_3Mo_3S_4)U(O^tBu)_3$** at −30 °C (Fig. 4 and Table 1; see Table S1† for structural parameters). The coordination environment of uranium is composed of the three sulfide atoms on the face of the hemi-cubane scaffold and three *tert*-butoxide ligands. The U–O distances are 2.079(3), 2.088(3), and 2.092(3) Å, which are slightly shorter compared to those observed in **$(Cp^*_3Mo_3S_4)Cp^*U(OPh)_2$**, likely due to the electronic influence of the substituents on uranium and/or the coordination number of uranium. However, the U–O distances closely resemble those of U(IV) *tert*-butoxide complexes reported in the literature, such as $[Li(THF)]_2[U^{4+}(O^tBu)_6]$ (U–O = 2.137(9), 2.140(8) Å), $[U^{4+}(O^tBu)_4(py)_2]$ (U–O = 2.115(3), 2.130(2) Å), and $[(C_5Me_5)_2U(O^tBu)(SePh)]$ (U–O = 2.029(6) Å).[57–59] The Mo–μS_U (avg) distance is 2.385(4) Å, which closely resembles that observed in the bis-hydroxide and bis-phenoxide compounds (2.370(2) Å and 2.374(4) Å, respectively). The

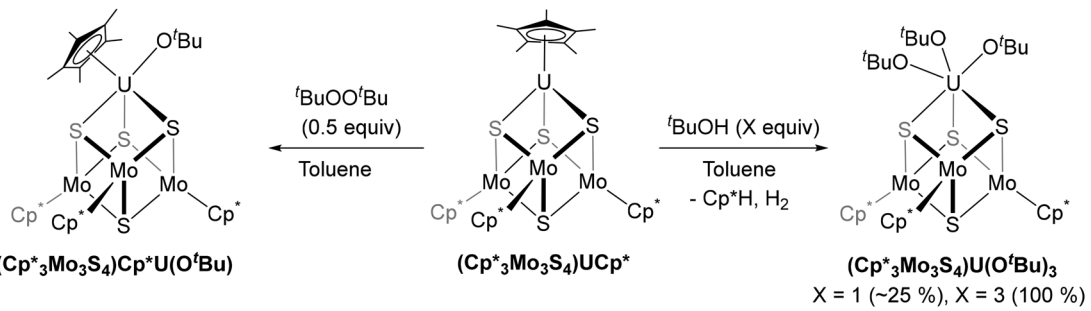

Scheme 4 Synthesis of **$(Cp^*_3Mo_3S_4)Cp^*U(O^tBu)$** and **$(Cp^*_3Mo_3S_4)U(O^tBu)_3$**.

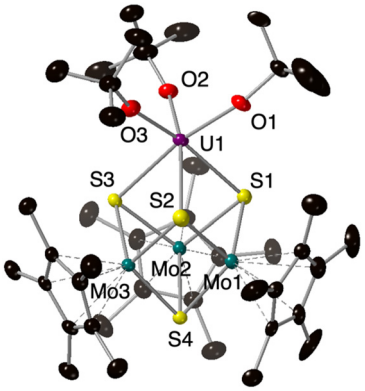

Fig. 4 Molecular structure of [$(Cp^*_3Mo_3S_4)U(O^tBu)_3$] shown with 40% probability ellipsoids. Hydrogen atoms have been removed for clarity. Key: black, C; red, O; yellow, S; teal, Mo; purple, U.

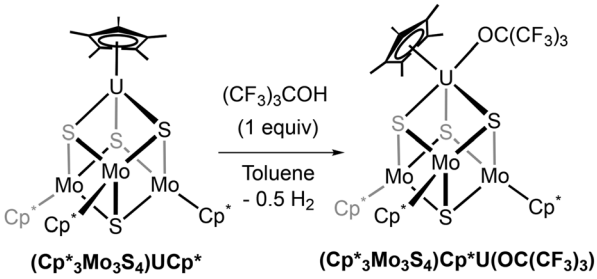

Scheme 5 Synthesis of $(Cp^*_3Mo_3S_4)Cp^*U(OC(CF_3)_3)$.

$U–S_{surf}$ distance is 1.8208(7) Å. The ∠U–O–C in $(Cp_3Mo_3S_4)U(O^tBu)_3$ range from 157.4(3)° to 162.2(2)°, showing a smaller angle compared to literature-known examples (162.4(4)° to 176.8(7)°).[57–59] The smaller ∠U–O–C in $(Cp_3Mo_3S_4)U(O^tBu)_3$ are most likely due to the steric bulk of the metalloligand.

Intrigued by this observation, we sought to synthesize the mono-*tert*-butoxide species through an alternative pathway to investigate whether the steric bulk of the *tert*-butyl group or the pK_a of the –OH proton alters the reactivity. In the context of forming uranium mono-alkoxide compounds, Meyer and co-workers recently reported the reactivity of low-valent uranium with peroxides.[60] Moreover, the precedence of the reactivity study of low-valent uranium precursor $UTp^{Me2}I_2(thf)_2$ with 0.5 equivalent of di-*tert*-butyl peroxide suggests the formation of corresponding mono-*tert*-butoxide complex $[UTp^{Me2}I_2(O^tBu)]$.[61] These reports prompted us to investigate the reactivity of our fully reduced cluster with peroxides, aiming to synthesize $(Cp^*_3Mo_3S_4)Cp^*U(O^tBu)$, which could not be accessed through uranium-metalloligand cooperative O–H bond activation of *tert*-butanol (Scheme 4). Our attempt involved the reaction of $(Cp^*_3Mo_3S_4)UCp^*$ with 0.5 equivalent of di-*tert*-butyl peroxide, which reacted immediately, as observed by ^{1}H NMR spectroscopy (Fig. S16†). The spectrum indicated the formation of a single product, with the Mo–Cp* (4.51 ppm) and U–Cp* (−3.26 ppm) methyl proton resonances shifted downfield compared to $(Cp^*_3Mo_3S_4)UCp^*$. These resonances closely resemble those observed for mono-methoxide and phenoxide species. Additionally, a resonance was observed at 36.65 ppm, which is assigned to *tert*-butyl protons. The intensity ratio of 45 : 15 : 9 suggests the formation of $(Cp^*_3Mo_3S_4)Cp^*U(O^tBu)$, which had only been observed as a minor product in the reaction with one equivalent of *tert*-butanol (Fig. S17†). Access to the mono-*tert*-butoxide species through this alternative pathway further substantiates the role of the pK_a of the alcohol –OH group in the reactivity of the uranium-doped thiomolybdate cluster.

A final substrate was explored to definitively rule out steric effects of the alcohol substrate as the determinate of reactivity. Toward this goal, nonafluoro-*tert*-butanol was selected as a suitable substrate, given its steric bulk and low pK_a of the –OH proton.[62,63] The reaction of $(Cp^*_3Mo_3S_4)UCp^*$ with one equivalent of nonafluoro-*tert*-butanol results in immediate consumption of the starting material and liberation of H_2, as observed in the ^{1}H NMR spectrum, indicating reduction of the alcohol (Scheme 5 and Fig. S18†). Additionally, the downfield shift of both the Cp*-methyl protons on molybdenum (4.21 ppm) and uranium (8.12 ppm) in the ^{1}H NMR spectrum is consistent with oxidation of the cluster. Furthermore, the trend of downfield shifts for the Cp*-methyl protons on uranium upon introducing increasingly electron-withdrawing substituents on uranium in the mono-alkoxide compounds [$(Cp^*_3Mo_3S_4)Cp^*U(OR)$; R = Me, Ph, Ph^{Cl2}] is noted, supporting the formation of the expected mono-alkoxide compound. The ^{19}F signal of $U–OC(CF_3)_3$ was observed at −87.15 ppm (Fig. S19†); the ^{19}F chemical shift of the $–CF_3$ group closely matches that reported for the analogous $Cp_3U(IV)(OC(CF_3)_2(CCl_3))$ compound; −97.1 ppm.[64] Based on these results, the product is assigned as $(Cp^*_3Mo_3S_4)UCp^*(OC(CF_3)_3)$. Formation of the mono-alkoxide derivative provides conclusive support for the pK_a of the substrate determining the pathway of reactivity at the uranium-substituted thiomolybdate cluster.

Conclusions

In summary, this work explores the reactivity of low-valent uranium supported by a redox-active molybdenum sulfide metalloligand $(Cp^*_3Mo_3S_4)UCp^*$ toward a range of alcohols with varying pK_a values for the –OH proton. We demonstrate that uranium and the metalloligand operate cooperatively in activating alcohols, as observed with water in our previous report. The reactivity of different alcohols, including methanol, phenol, 2,6-dichlorophenol, and *tert*-butanol was studied, which afforded the corresponding uranium mono-alkoxide clusters *via* uranium-metalloligand cooperative activation of the O–H bond. In contrast, the reaction with *tert*-butanol led to protonolysis of the Cp* ligand, yielding a uranium tris-*tert*-butoxide cluster. Based on the trend in alcohol pK_a values (^{t}BuOH > MeOH > PhOH > $PhCl_2OH$ > $HOC(CF_3)_3$), we propose that a significant increase in the pK_a of the alcohol's –OH

proton favors Cp* protonolysis. This conclusion is supported by the independent synthesis of the uranium-mono-*tert*-butoxide cluster through an alternative route involving the reaction with di-*tert*-butyl peroxide.

Author contributions

K. P. conceived of the project and synthesized and characterized all compounds. W. W. B. determined the crystal structures of the compounds reported. E. M. M. directed the project. The manuscript was written through contributions of all authors. All authors have given approval to the final version of the manuscript.

Data availability

The data supporting this article have been included as part of the ESI.† Crystallographic data for have been deposited at the CCDC (2388772–2388775).†

Conflicts of interest

There are no conflicts to declare.

Acknowledgements

This research was funded by the U.S. Department of Energy, Office of Basic Energy Sciences through the Heavy Element Program (DE-SC0020436). E. M. M. is the recipient of a Camille Dreyfus Teacher-Scholar Award, which has provided additional resources to support this research.

References

1 A. R. Fox, S. C. Bart, K. Meyer and C. C. Cummins, *Nature*, 2008, **455**, 341.
2 D. R. Hartline and K. Meyer, *JACS Au*, 2021, **1**, 698–709.
3 F. Haber and R. Le Rossignol, *Process of Making Ammonia*, US999025A, 1910.
4 J. Leduc, M. Frank, L. Jürgensen, D. Graf, A. Raauf and S. Mathur, *ACS Catal.*, 2019, **9**, 4719–4741.
5 O. T. Summerscales and F. G. N. Cloke, in *Organometallic and Coordination Chemistry of the Actinides*, ed. T. E. Albrecht-Schmitt, Springer Berlin Heidelberg, Berlin, Heidelberg, 2008, pp. 87–117. DOI: 10.1007/430_2007_078.
6 C. Deng, J. Liang, R. Sun, Y. Wang, P.-X. Fu, B.-W. Wang, S. Gao and W. Huang, *Nat. Commun.*, 2023, **14**, 4657.
7 J. Su, W.-L. Li, G. V. Lopez, T. Jian, G.-J. Cao, W.-L. Li, W. H. E. Schwarz, L.-S. Wang and J. Li, *J. Phys. Chem. A*, 2016, **120**, 1084–1096.
8 S. Fortier, N. Kaltsoyannis, G. Wu and T. W. Hayton, *J. Am. Chem. Soc.*, 2011, **133**, 14224–14227.
9 D. K. Modder, C. T. Palumbo, I. Douair, F. Fadaei-Tirani, L. Maron and M. Mazzanti, *Angew. Chem., Int. Ed.*, 2021, **60**, 3737–3744.
10 L. Barluzzi, S. R. Giblin, A. Mansikkamäki and R. A. Layfield, *J. Am. Chem. Soc.*, 2022, **144**, 18229–18233.
11 E. Lu and S. T. Liddle, *Dalton Trans.*, 2015, **44**, 12924–12941.
12 M. J. Polinski, P. C. Burns and T. Albrecht-Schmitt, in *Comprehensive Inorganic Chemistry II*, ed. J. Reedijk and K. Poeppelmeier, Elsevier, Amsterdam, 2nd edn, 2013, pp. 601–610.
13 H. Idriss, *Surf. Sci. Rep.*, 2010, **65**, 67–109.
14 S. J. Kraft, P. E. Fanwick and S. C. Bart, *J. Am. Chem. Soc.*, 2012, **134**, 6160.
15 N. H. Anderson, S. O. Odoh, Y. Yao, U. J. Williams, B. A. Schaefer, J. J. Kiernicki, A. J. Lewis, M. D. Goshert, P. E. Fanwick, E. J. Schelter, J. R. Walensky, L. Gagliardi and S. C. Bart, *Nat. Chem.*, 2014, **6**, 919–926.
16 J. J. Kiernicki, B. S. Newell, E. M. Matson, N. H. Anderson, P. E. Fanwick, M. P. Shores and S. C. Bart, *Inorg. Chem.*, 2014, **53**, 3730–3741.
17 N. H. Anderson, S. O. Odoh, U. J. Williams, A. J. Lewis, G. L. Wagner, J. Lezama Pacheco, S. A. Kozimor, L. Gagliardi, E. J. Schelter and S. C. Bart, *J. Am. Chem. Soc.*, 2015, **137**, 4690–4700.
18 S. J. Kraft, P. E. Fanwick and S. C. Bart, *Inorg. Chem.*, 2010, **49**, 1103–1110.
19 M. D. Straub, E. T. Ouellette, M. A. Boreen, R. D. Britt, K. Chakarawet, I. Douair, C. A. Gould, L. Maron, I. Del Rosal, D. Villarreal, S. G. Minasian and J. Arnold, *J. Am. Chem. Soc.*, 2021, **143**, 19748–19760.
20 M. A. Boreen and J. Arnold, *Dalton Trans.*, 2020, **49**, 15124–15138.
21 D. K. Modder, C. T. Palumbo, I. Douair, R. Scopelliti, L. Maron and M. Mazzanti, *Chem. Sci.*, 2021, **12**, 6153–6158.
22 S. R. Chowdhury, C. A. P. Goodwin and B. Vlaisavljevich, *Chem. Sci.*, 2024, **15**, 1810–1819.
23 M. D. Straub, S. Hohloch, S. G. Minasian and J. Arnold, *Dalton Trans.*, 2018, **47**, 1772–1776.
24 S. T. Liddle, *Coord. Chem. Rev.*, 2015, **293–294**, 211–227.
25 S. Fortier, J. R. Aguilar-Calderón, B. Vlaisavljevich, A. J. Metta-Magaña, A. G. Goos and C. E. Botez, *Organometallics*, 2017, **36**, 4591–4599.
26 H. S. La Pierre, H. Kameo, D. P. Halter, F. W. Heinemann and K. Meyer, *Angew. Chem., Int. Ed.*, 2014, **53**, 7154–7157.
27 N. Jori, M. Falcone, R. Scopelliti and M. Mazzanti, *Organometallics*, 2020, **39**, 1590–1601.
28 C. Camp, J. Andrez, J. Pécaut and M. Mazzanti, *Inorg. Chem.*, 2013, **52**, 7078–7086.
29 J. J. Kiernicki, R. F. Higgins, S. J. Kraft, M. Zeller, M. P. Shores and S. C. Bart, *Inorg. Chem.*, 2016, **55**, 11854–11866.
30 K. Patra, W. W. Brennessel and E. M. Matson, *J. Am. Chem. Soc.*, 2024, **146**, 20147–20157.
31 D. P. Halter, F. W. Heinemann, J. Bachmann and K. Meyer, *Nature*, 2016, **530**, 317.

32 D. P. Halter, F. W. Heinemann, L. Maron and K. Meyer, *Nat. Chem.*, 2018, **10**, 259–267.
33 X. Zhao, L. Bai, J. Li and X. Jiang, *J. Am. Chem. Soc.*, 2024, **146**, 11173–11180.
34 R. H. Harris, V. J. Boyd, G. J. Hutchings and S. H. Taylor, *Catal. Lett.*, 2002, **78**, 369–372.
35 M. Liu, H. Chen, X. Tang, H. Liu, B. Tu, W. Guo, Y. Zheng, Y. Liu, Y. Tang, R. He and W. Zhu, *Small*, 2022, **18**, 2107444.
36 S. T. Löffler, J. Hümmer, A. Scheurer, F. W. Heinemann and K. Meyer, *Chem. Sci.*, 2022, **13**, 11341–11351.
37 M. W. Rosenzweig, J. Hümmer, A. Scheurer, C. A. Lamsfus, F. W. Heinemann, L. Maron, M. Mazzanti and K. Meyer, *Dalton Trans.*, 2019, **48**, 10853–10864.
38 H. I. Karunadasa, E. Montalvo, Y. Sun, M. Majda, J. R. Long and C. J. Chang, *Science*, 2012, **335**, 698–702.
39 Z. Huang, W. Luo, L. Ma, M. Yu, X. Ren, M. He, S. Polen, K. Click, B. Garrett, J. Lu, K. Amine, C. Hadad, W. Chen, A. Asthagiri and Y. Wu, *Angew. Chem., Int. Ed.*, 2015, **54**, 15181–15185.
40 B. R. Garrett, S. M. Polen, K. A. Click, M. He, Z. Huang, C. M. Hadad and Y. Wu, *Inorg. Chem.*, 2016, **55**, 3960–3966.
41 Y. Yan, B. Xia, Z. Xu and X. Wang, *ACS Catal.*, 2014, **4**, 1693–1705.
42 K. Patra, W. W. Brennessel and E. M. Matson, *Chem. Commun.*, 2024, **60**, 530–533.
43 G. M. Sheldrick, *Acta Crystallogr., Sect. A: Found. Adv.*, 2015, **71**, 3–8.
44 G. M. Sheldrick, *Acta Crystallogr., Sect. C: Struct. Chem.*, 2015, **71**, 3–8.
45 B. Kosog, H. S. La Pierre, M. A. Denecke, F. W. Heinemann and K. Meyer, *Inorg. Chem.*, 2012, **51**, 7940–7944.
46 L. Karmazin, M. Mazzanti and J. Pécaut, *Inorg. Chem.*, 2003, **42**, 5900–5908.
47 Y. Ohki, K. Uchida, M. Tada, R. E. Cramer, T. Ogura and T. Ohta, *Nat. Commun.*, 2018, **9**, 3200.
48 H. S. La Pierre, A. Scheurer, F. W. Heinemann, W. Hieringer and K. Meyer, *Angew. Chem., Int. Ed.*, 2014, **53**, 7158–7162.
49 B. Delavaus-Nicot and M. Ephritikhine, *J. Organomet. Chem.*, 1990, **399**, 77–82.
50 D. S. J. Arney and C. J. Burns, *J. Am. Chem. Soc.*, 1993, **115**, 9840–9841.
51 J. J. Kiernicki, S. L. Staun, M. Zeller and S. C. Bart, *Organometallics*, 2017, **36**, 665–672.
52 R. K. Thomson, C. R. Graves, B. L. Scott and J. L. Kiplinger, *Eur. J. Inorg. Chem.*, 2009, **2009**, 1451–1455.
53 D. D. Schnaars, G. Wu and T. W. Hayton, *Dalton Trans.*, 2009, 3681–3687, DOI: **10.1039/B823002A**.
54 I. Takei, K. Suzuki, Y. Enta, K. Dohki, T. Suzuki, Y. Mizobe and M. Hidai, *Organometallics*, 2003, **22**, 1790–1792.
55 F. Muller and L. Caillard, in *Ullmann's Encyclopedia of Industrial Chemistry*, 2011, DOI: **10.1002/14356007.a07_001.pub2**.
56 Y. Zeng, X. Chen, D. Zhao, H. Li, Y. Zhang and X. Xiao, *Fluid Phase Equilib.*, 2012, **313**, 148–155.
57 S. Fortier, G. Wu and T. W. Hayton, *Inorg. Chem.*, 2008, **47**, 4752–4761.
58 A. Lichtenberg, A. Lichtenberg, M. Pieper and S. Mathur, *Eur. J. Inorg. Chem.*, 2024, **27**, e202300474.
59 R. K. Thomson, C. R. Graves, B. L. Scott and J. L. Kiplinger, *J. Chem. Crystallogr.*, 2011, **41**, 1241–1244.
60 D. R. Hartline, S. T. Löffler, D. Fehn, J. M. Kasper, F. W. Heinemann, P. Yang, E. R. Batista and K. Meyer, *J. Am. Chem. Soc.*, 2023, **145**, 8927–8938.
61 J. P. Leal, N. Marques and J. Takats, *J. Organomet. Chem.*, 2001, **632**, 209–214.
62 W. N. Olmstead, Z. Margolin and F. G. Bordwell, *J. Org. Chem.*, 1980, **45**, 3295–3299.
63 R. Filler and R. M. Schure, *J. Org. Chem.*, 1967, **32**, 1217–1219.
64 F. Knösel, H. W. Roesky and F. Edelmann, *Inorg. Chim. Acta*, 1987, **139**, 187–188.